

Grating Diffraction Effects in the THz Domain

J.-L. COUTAZ^{a,*}, F. GARET^a, E. BONNET^b, A.V. TISHCHENKO^b,
O. PARRIAUX^b AND M. NAZAROV^c

^aLAHC, University of Savoie, 73 367 Le Bourget du Lac Cedex, France

^bLTSI, University Jean Monnet, 42 000 Saint-Etienne, France

^cInternational Laser Center, Moscow State University, Moscow, Russia

We study the far infrared electromagnetic response of grating devices by THz time-domain spectroscopy. We first show that THz waves are efficiently injected into silicon waveguides using grating couplers. Moreover, changing the waveguide material parameters by white-light illumination allows us to strongly modify the coupling efficiency. Then we demonstrate resonant effects in segmented grating structures that act as perfect mirrors at selected wavelengths even for focused beams. About 10 periods of the grating participate in the phenomenon, nevertheless the resonance frequency width of the device remains narrow. This collection of experiments shows that millimeter-size mock-ups and THz waves can be effectively used to extrapolate the optical response of micron-size actual devices.

PACS numbers: 78.47.+p, 72.30.+q, 42.65.Re

1. Introduction

Among the numerous applications [1] of electromagnetic waves belonging to the terahertz (THz) domain, it is possible to measure the electromagnetic response of mock-ups of much larger or smaller sizes than the actual related items. THz wavelengths corresponding to the strongest part of the spectrum of optoelectronics-generated ultrashort pulses are typically ranging from 100 μm (3 THz) to 1 mm (300 GHz). On the one hand, they are 20–60 smaller than radar wavelengths and thus they allow studying the radar signature of mock-ups that are as smaller as compared to actual equipments. This has been applied successfully by Grischkowsky and his group [2] to study the radar signature of military airplanes. On the other hand, THz wavelengths are about 1000 times larger than

*corresponding author; e-mail: coutaz@univ-savoie.fr

optical wavelengths, and they can be used to study the response of millimeter-sized mock-ups that are much easier to manufacture than actual micron-sized optical devices. This technique has been already employed to demonstrate the first 3D photonic crystals, as the pioneering work in the GHz domain [3], or even in the THz domain [4, 5].

In this paper, we apply this technique to characterize grating devices with millimeter groove periodicity that can be made with mechanical tools, while the fabrication of related optical devices is more difficult. In particular, we study wavelength-selected filters made of segmented air–silicon waveguide, which are almost impossible to fabricate with dimensions designed for the optical domain. In the first part of the paper, we report on the use of diffraction gratings as couplers of the incoming THz beam into dielectric silicon waveguides. We derive the propagation properties of the waveguide from the measured diffraction pattern. We show that it is possible to change the coupling efficiency by varying the waveguide material characteristics, for example by exciting carriers via white-light illumination of the device. In the second part of the paper, we are interested in the diffraction properties of segmented waveguides that are made of parallel silicon rods of rectangular section located in air. The device corresponds to a 1D photonic band-gap crystal or to a dielectric grid grating for millimeter waves. We show that this device exhibits amazing diffraction properties, especially for focused beams. For both types of experiments, i.e. coupling into waveguides and frequency-selective mirrors, diffraction effects take place when the grating periodicity is of the order of the THz wavelength. Therefore, this work has required grating devices with sub-millimeter periodicity, whose fabrication could be done without microelectronics technology.

2. Experiments

All the experimental data reported in this paper were recorded using a classical THz time-domain spectroscopy setup [6]. The emitting and receiving antennae are LTG-GaAs photoswitches excited with 100 fs duration pulses at 800 nm delivered by a 82 MHz repetition rate Ti:sapphire mode-locked laser. The setup radiates picosecond electromagnetic bursts whose spectrum ranges from 0.1 up to 4 THz. The signals are recorded over a 150 ps time-window, corresponding to a frequency resolution of ≈ 6 GHz. The quasi-optics THz system includes hemispheric silicon domes attached to the photoswitches, and 4 parabolic mirrors. The waist of the THz beam is located in position A (see Fig. 1), and its diameter is 4 mm at ≈ 600 GHz (convergence angle $\approx 2 \times 6^\circ$). In between the two first parabolic mirrors (position B), the beam is parallel with a diameter of about 5 cm. Thus putting the grating device either in A or in B allows us to perform measurements respectively with focused or parallel THz beams.

The grating coupler consists of a high resistivity *n*-type free-standing silicon wafer (2 k Ω cm) that serves as waveguide for THz waves, at top of which

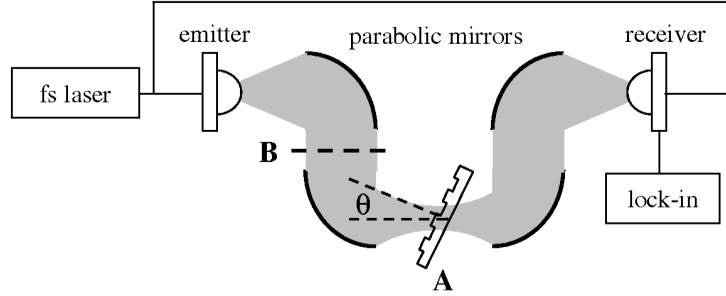


Fig. 1. THz time-domain setup.

we engraved parallel rectangularly-shaped grooves using a diamond dicing saw. The wafer thickness is $d_w = 210 \mu\text{m}$ and its refractive index and the absorption, measured prior to grating fabrication by THz time-domain spectroscopy, are respectively equal to 3.4 and less than 2 cm^{-1} over the whole range 0.1–2 THz. The grating geometrical parameters were measured with a Talystep surface profiler: the periodicity d is $322 \mu\text{m}$, the groove depth δ is $20 \mu\text{m}$ and the groove width is $142 \mu\text{m}$ (filling factor $\approx 45\%$).

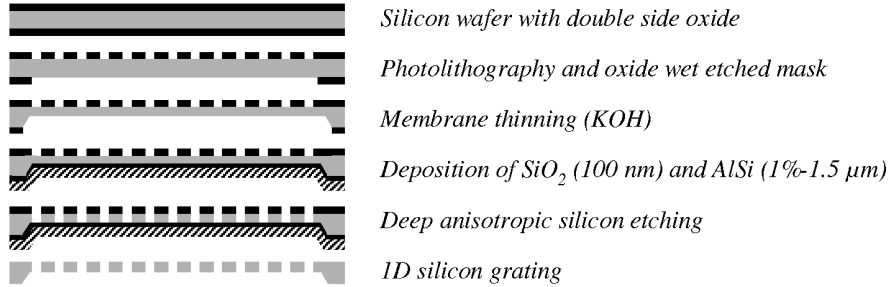


Fig. 2. Schematic of the fabrication process flow for a 1D silicon grating.

The fabrication of the segmented waveguide is more delicate. We used a $525 \mu\text{m}$ thick high resistivity ($8 \text{ k}\Omega \text{ cm}$) silicon wafer with a $2 \mu\text{m}$ oxide layer at each side, which is then covered by a photoresist film. The grating drawing ($d = 385 \mu\text{m}$) is realized with a direct laser-writer system, and then the front oxide mask is wet-etched. The second fabrication step consists in thinning down to $d_w = 210 \mu\text{m}$ the silicon wafer with KOH, the front side being protected. Finally, deep anisotropic silicon etching is performed following the ‘‘Bosch’’ process. Figure 2 represents the schematic process flow to obtain a 1D silicon grating suspended in air, including intermediate fabrication stages not described here. Figure 3a shows a picture of the $4''$ silicon wafer in which 3 gratings were processed. The one used in this work is $1.5 \times 7 \text{ cm}^2$ wide. Figure 3b presents an enlarged view of the rectangular silicon rods.

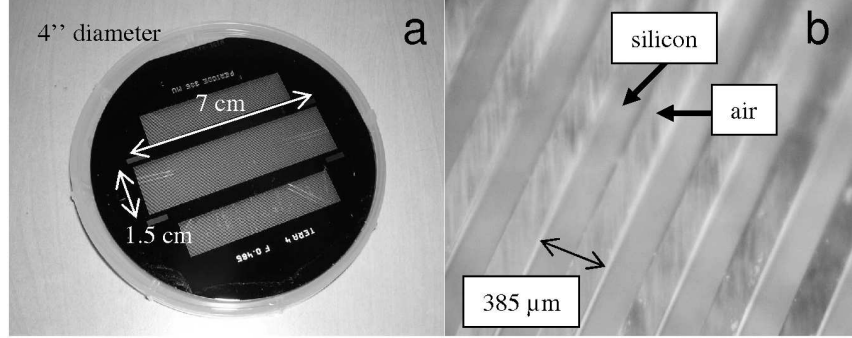


Fig. 3. Photography of the 1D grating device: (a) overall device, (b) zoom.

3. Principles and theoretical approach

The coupling of the incoming beam into the waveguide occurs when the condition of conservation of the parallel wave vector component is satisfied (Fig. 4a):

$$k_i'' + m k_{\text{grat}} = \frac{2\pi f}{c} \sin \theta + m \frac{2\pi}{d} = k_{\text{guided}}^{(p)} = \frac{2\pi f}{c} n_{\text{eff}}^{(p)}, \quad (1)$$

where $k_{\text{grat}} = 2\pi/d$ is the wave vector associated to the grating, m is the order of diffraction, $n_{\text{eff}}^{(p)}$ is the effective index of the guided mode p , $c = 3 \times 10^8$ m/s, f is the THz frequency and θ is the angle of incidence (see Fig. 1). In the case of grating coupler, we measure the signal transmitted in the 0-order of diffraction (black arrow in Fig. 4b). Each time Eq. (1) is fulfilled, a guided mode is excited. The transmitted signal results from the interference between the directly transmitted beam and the guided light that is out-diffracted by the grating in the 0-order direction (Fig. 4c). As the guided light suffers losses (absorption of the waveguide material, scattering by defects), energy is missing in transmission and dark lines (the so-called “m-lines”) are observed. When Eq. (1) is not fulfilled, the incident beam does not interact resonantly with the grating: the device behaves as a parallel slab and we observe classical Fabry–Perot patterns in transmission. We have calculated the diffraction efficiency of this grating coupler using the differential method [7], which is well-adapted to dielectric gratings. As known in optics, the

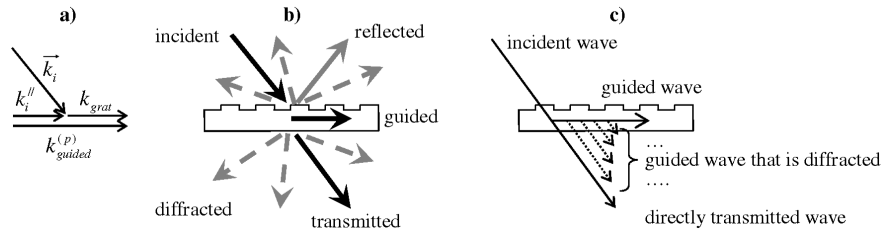


Fig. 4. Diffraction processes in a grating coupler: (a) momentum conservation, (b) overall diffraction phenomenon, (c) transmission signal in the 0-order of diffraction.

optimum coupling is achieved when the groove depth is roughly one tenth of the period.

The segmented grating acts as a frequency-selective mirror based on the resonant reflection [8] which results from destructive interferences taking place in the device. Under coupling condition (1), part of the incident beam is directly transmitted through the device (t in Fig. 5a), while the other part is firstly guided in the structure and then is diffracted out (s in Fig. 5a). The interference is fully destructive when these two parts t and s are equal in modulus and opposite in phase. This condition is fulfilled when the product of the incident beam width by the grating radiation coefficient α is much larger[†] than 1. In this case, the incident beam is totally reflected by the device and no light is transmitted throughout. In the case of normal incidence (Fig. 5b), co- and contra-propagating guided waves are equally excited through the ± 1 orders of diffraction of the grating. The guided waves are diffracted out via the ± 1 orders of diffraction and are retro-coupled via the ± 2 orders of diffraction. This phenomenon occurs when the wave vectors obey the following laws:

$$\begin{cases} k_i'' + (\pm 1)k_{\text{grat}} = (\pm 1)k_{\text{guided}}^{(p)} & \text{in- and out-coupling condition,} \\ (\pm 1)k_{\text{guided}}^{(p)} + (\mp 2)k_{\text{grat}} = (\mp 1)k_{\text{guided}}^{(p)} & \text{retro-coupling condition.} \end{cases} \quad (2)$$

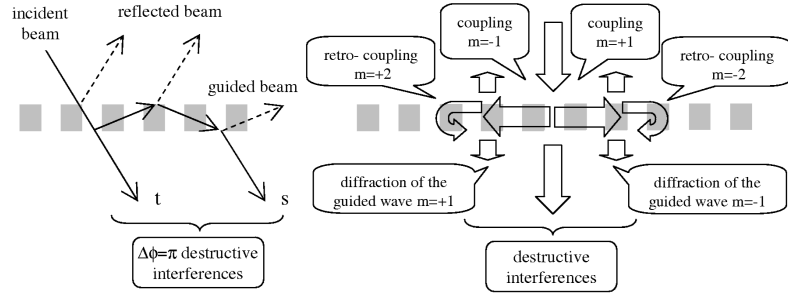


Fig. 5. Resonant diffraction effect in the 1D segmented grating: (a) oblique incidence, (b) case of normal incidence.

Let us notice that relations (2) are both verified when $k_{\text{grat}} = k_{\text{guided}}^{(p)}$. From a practical point of view, the present device shows a narrow spectral width due to a small radiation coefficient α whereas a large second-order coupling coefficient κ ensures a tight confinement of the coupled wave under the incident beam, which amounts to a wide angular aperture. A large κ value is achieved with a segmented grating made of an alternative stack of high and low index materials (here silicon ($n_{\text{Si}} \approx 3.4$) and air ($n_{\text{air}} = 1$)), which exhibits a large second-order Fourier

[†] Due to the out-diffraction, the guided light intensity decreases exponentially along the waveguide. The grating radiation coefficient is equal to the inverse of the $1/e$ decay length of the guided amplitude.

coefficient, while a low α value is obtained by adjusting the thickness d_w of the structure [9]. The device electromagnetic response was simulated with a FDTD code.

4. Grating-assisted coupling of THz waves into a dielectric waveguide

Figure 6 shows the measured coefficient of transmission of the grating coupler for both TE and TM polarizations recorded at normal incidence. The continuous lines are calculated with the differential method, without any variable parameter, since the geometrical parameters are known from the fabrication process and the silicon refractive index was measured previously by THz time-domain spectroscopy. We clearly observe large oscillations with an approximate periodicity of 200 GHz, which correspond to the Fabry–Perot resonances of the device. At selected frequencies, relation (1) is fulfilled and thus narrow absorption peaks (m-lines) appear because of the excitation of guided modes. The frequency width of the peaks is more often not resolved because of the rather low experimental resolution (6 GHz). Nevertheless, the transmission can be as low as 5% (2.5% in energy) at 520 GHz (TM), which demonstrates the efficiency of the device.

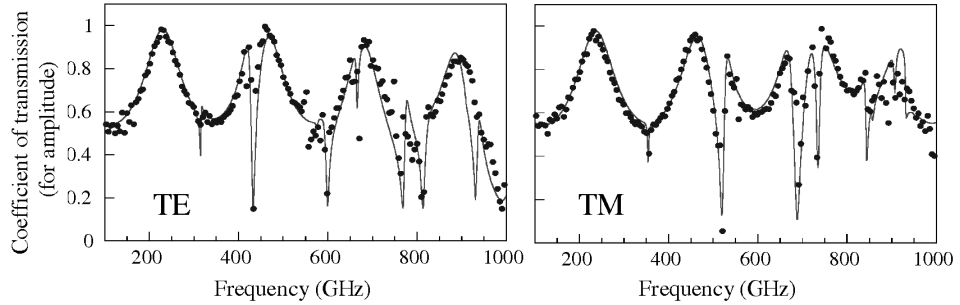


Fig. 6. Coefficient of transmission for field amplitude (TE and TM polarizations). Dots are measured data, continuous lines are calculated with the differential method.

THz time-domain spectroscopy allows us to measure the phase of the signals, which is more difficult in optics. To clearly show any detail of the phase dispersion curve (Fig. 7), we define the effective optical thickness d_{eff} of the device, which is related to the phase $\Delta\varphi$ of its transmission coefficient by

$$\Delta\varphi \equiv \frac{2\pi f}{c} d_{\text{eff}}. \quad (3)$$

This permits us to get rid of the large variation of frequency over the whole recorded spectrum, which hides any small variation of the phase. The Fabry–Perot oscillations are still observed in Fig. 7, while a phase jump occurs at each resonant coupling. All the measurements were repeated for several angles of incidence. From the frequency position of each m-line and the knowledge of the angle of incidence, we determine the effective index of the guided mode p as well

as the coupling order m using relation (1). In fact, to be sure to associate without ambiguity the actual mode number p and coupling order m to each observed m-line, we have simultaneously calculated the guided mode dispersion of a parallel slab silicon waveguide whose thickness ($201 \mu\text{m}$) is equal to the sum of the homogeneous waveguide thickness and half the corrugated region thickness [10]. Both experimental data and theoretical curves (planar waveguide) are presented in Fig. 8 and are in very good agreement, excepted for selected frequencies (for example at 700 GHz for the TE_2 mode) at which dispersion curves of the periodic structure cross and repeal, leading to forbidden frequency band gaps. In this case, the flat slab waveguide approximation is not valid.

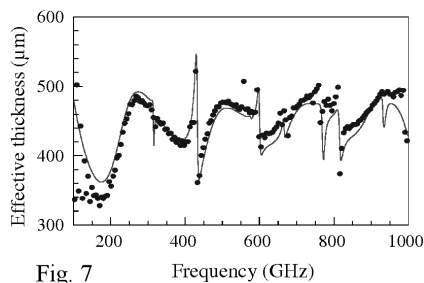


Fig. 7

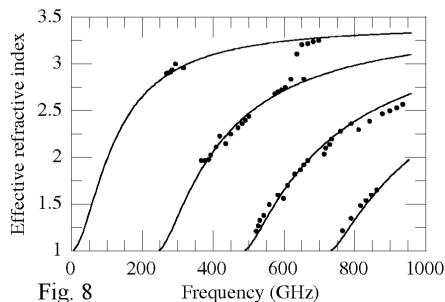


Fig. 8

Fig. 7. Effective thickness versus frequency in TE polarization. Dots are measured data, continuous lines are calculated with the differential method.

Fig. 8. Dispersion of the guided mode of a silicon waveguide in the THz domain. Dots are experimental data. Continuous lines are calculated for a $201 \mu\text{m}$ thick parallel slab.

It is well known that the refractive index and absorption coefficient of a semiconductor depends strongly on its free carrier density. It is particularly verified in the far infrared, as there is no residual effect of inter- and intraband transitions: thus semiconductor electromagnetic response is well described by a free electron gas model, like the Drude one [11]. Therefore, the silicon grating coupler efficiency can be tuned by changing the silicon material properties through the variation of its free carrier concentration. The carrier injection is easily achieved via light-illumination of the whole device. Even if light absorption occurs only within a few microns at the wafer surface, the long free carrier lifetime in intrinsic silicon permits an efficient diffusion of the carriers into the whole slab, leading to a homogeneous carrier density distribution.

Figure 9 shows the refractive index and absorption coefficient of intrinsic silicon. The refractive index is almost constant over the 0.2–1.5 THz range, while the absorption coefficient is small, at the limit of sensitivity of our system. Under illumination, the refractive index decreases and the absorption coefficient increases strongly, showing a large dispersion in the THz range. This behavior is due to the photoexcited free carriers, as demonstrated by the good fit to the Drude model [12].

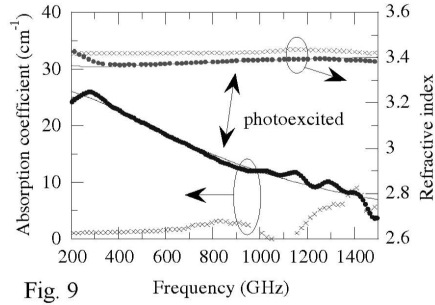


Fig. 9

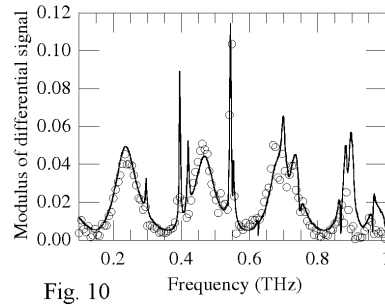


Fig. 10

Fig. 9. Refractive index and absorption coefficient of intrinsic silicon (crosses) and under illumination (full dots). The continuous lines are a fit using the Drude model.

Fig. 10. Photoinduced variation of the transmission of the silicon grating coupler. The continuous line is the theoretical curve calculated with the differential method.

Figure 10 presents the variation of transmission of the grating coupler device induced by illumination with white light. The white-light source is a tungsten lamp delivering an almost parallel beam with 1 W/cm^2 at the device. The white-light beam is chopped and impinges the device at normal incidence. A lock-in amplifier records the differential THz signal at the chopper frequency, i.e. the difference of transmission with and without illumination. When a THz guided mode is excited, the photoinduced variation is enhanced, as the THz wave propagates in a longer amount of silicon. At 540 GHz, the variation of transmission reaches 20.5% (41% in power). The experimental data are well fitted using the differential theory, in which the illuminated silicon parameters are obtained with the Drude model using 10^{14} cm^{-3} as carrier density. This density can be retrieved from the optical carrier injection density if we assume a carrier lifetime of $1 \mu\text{s}$ [13].

5. Resonant effects at THz frequencies in segmented grating structures

The transmission spectrum of the segmented grating device is shown in Fig. 11a for parallel THz beam, and in Fig. 11b for focused THz beam, both being TE polarized. The curves exhibit the classical Fabry–Perot oscillations together with absorption peaks and other resonant features. These minima can be associated to guided modes, proving definitively that such a segmented structure can guide light. The dispersion of the guided modes appears clearly when one examines the positions of a specified m-line for different angles of incidence. However, the dispersion of some modes is rather weak and the corresponding m-line minimum appears at a constant frequency over a large range of angles of incidence, for example at 522 GHz (Fig. 11a).

Thus it is expected, for example at this 522 GHz frequency, that the transmission of a focused beam should be weak. This is definitively observed in Fig. 11b, where the transmission at 522 GHz is about 0.28 (i.e., 8% in power). Due to the lack of frequency resolution of our THz time-domain setup, the peaks of absorption

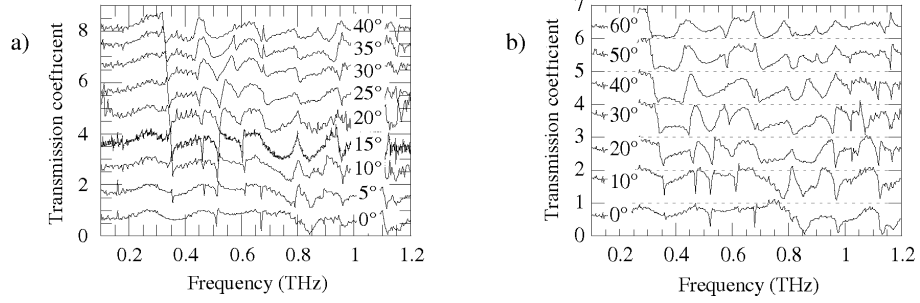


Fig. 11. Transmission coefficient of the segment grating versus frequency for different angles of incidence. Each plot has been shifted by 1 as compared to one below. (a) Parallel THz beam, (b) focused beam.

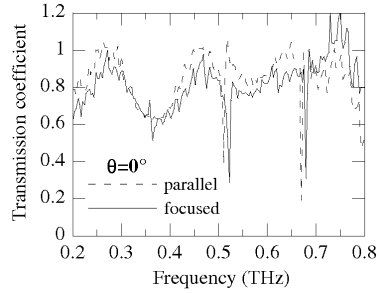


Fig. 12. Comparison of the transmission coefficient of the segmented grating in the case of parallel and focused THz beams at normal incidence.

are poorly resolved and the minimum value given here is certainly overestimated. Indeed, we already reported a transmission weaker than 1.2% for a similar structure [9]. Figure 12 compares the data recorded at normal incidence with focused and parallel beams. The slight difference of the frequency position of the m-lines could be due to a small misalignment ($< 2^\circ$) of the grating in the focused beam case. The minimum at 522 GHz is clearly distinguished. At 363 GHz (focused beam), one can see an m-line that does not exist in the parallel case. It originates from the contribution of all the wave vector components of the focused beam, for which a mode is excited at this frequency (see Fig. 11a for $\theta = 5^\circ, 10^\circ \dots$). Let us notice that, as the beam waist is about 4 mm at 600 GHz, only 10 grating grooves are shined and participate in the diffraction process.

The origin of the deep minima in transmission is questionable: is the explanation given in Sec. 3 right, or could we imagine other phenomena, like distribution of the transmitted light into other transmitted diffracted orders? This question is in part answered by measuring the signals transmitted and reflected in the 0-order by the device (see Fig. 13). The arrangement of our setup imposes an oblique incidence, i.e. $\theta = 45^\circ$. Moreover a reference for the reflected signal cannot be

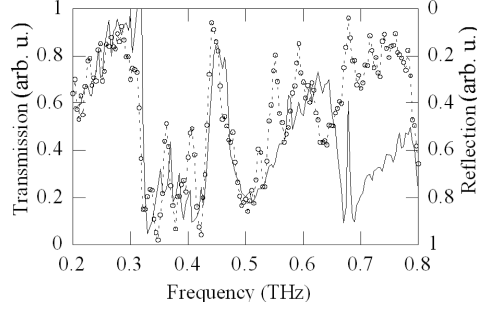


Fig. 13. Transmitted (continuous line) and reflected (dashed) THz signal at $\theta = 45^\circ$. The reflected signal is not calibrated to a reference signal, and thus data are given in arbitrary units.

measured, as it is in transmission, and thus the curves are given in arbitrary units. Nevertheless, one can see that from 0.2 up to 0.6 THz, both transmission and reflection are roughly complementary, i.e. they obey the following field conservation law:

$$r + t = A, \quad (4)$$

where r and t are respectively the amplitudes of the reflected and transmitted fields in the 0-order of diffraction. A is a constant that should tend to 1 in absence of absorption and scattering, but our relative measurements do not allow us to determine it.

We have tried to explain the origin, in terms of modes of propagation and diffraction orders, of each m-line shown in transmission (Fig. 11a) as we did for the grating coupler. Unfortunately, the differential method does not converge for the segmented grating structure. Nevertheless, for each incident angle, we can take the frequency position of the most remarkable minima of the transmission spectrum. Then, we deduce the wave vector of the excited mode using relation (1):

$$k_{\text{guided}}^{(p)} = k_i'' + m k_{\text{grat}} = \frac{2\pi f}{c} \sin \theta + m \frac{2\pi}{d}. \quad (5)$$

The unknown parameter is the diffraction order m . We choose m in such way that $k_{\text{guided}}^{(p)}$ belongs to the interval bounded by $k_{\text{guided}}^{\min} = \frac{2\pi f}{c} n_{\text{air}}$ and $k_{\text{guided}}^{\max} = \frac{2\pi f}{c} n_{\text{Si}}$. The data are shown in Fig. 14. Several values of m ($-2, -1, +1, +2$) lead to realistic solutions and, at this stage of the study, we cannot deduce which of these solutions is the right one. To progress towards the understanding of this diffraction phenomenon, we have supposed that, far from Bragg condition (i.e. retro-coupling through diffraction), each guided mode in the segmented waveguide propagates through an effective medium whose refractive index is: $n = \sqrt{(\varepsilon_{\text{Si}} + \varepsilon_{\text{air}})/2} = 2.51$. Thus we calculated the effective indices n_{eff} of the modes guided by a flat dielectric slab with $n = 2.51$ and a thickness $d_w = 210 \mu\text{m}$. Finally, we applied relation (1) to take into account coupling between co- and contra-propagating modes produced

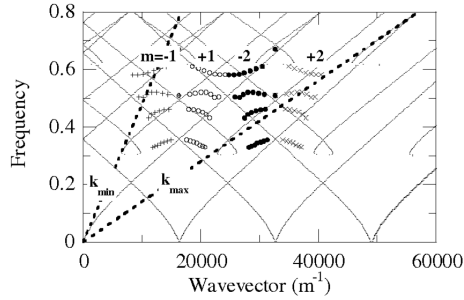


Fig. 14. Dispersion of the guided modes. The lines are the guided modes of a planar waveguide with $\varepsilon = 6.3$ (thickness $210 \mu\text{m}$), which are diffracted by the grating (see relation (5)). The dashed lines k_{\min} and k_{\max} correspond to the minimum and maximum values of the guided wave vector. The dots are the measured (from Fig. 12) parallel component of the incident wave vector to which is added m times the grating wave vector in order to take into account the grating-assisted coupling.

by grating diffraction. This implies that the grating disturbs weakly the guided modes, which is of course not the case here. Thus, this approach constitutes only a first attempt to understand the recorded transmission spectra. The theoretical curves are also plotted in Fig. 14. They show that the dispersion plot becomes very complicated, almost inextricable, when the frequency increases, due to the emergence of numerous higher modes. It is clearly seen that the parallel slab model does not give a good description of the experimental data. As anticipated, the dispersion properties of the segmented waveguide are strongly different from that of a planar homogeneous waveguide. Therefore, an adapted theory is necessary to fully describe the waveguiding properties of such segmented device.

6. Conclusion

We have shown that new and original results can be obtained by studying the electromagnetic response of millimeter-size devices in the THz domain. This can help in extrapolating the optical response of much smaller related items that are difficult to fabricate. In the present paper we have demonstrated coupling properties of gratings engraved at top of waveguides, as well as amazing diffraction properties of segmented gratings. The full study of such segmented gratings, especially their guiding properties, requires additional modeling works.

Acknowledgments

We acknowledge a support from the European Commission Center of Excellence in Processing, Research and Application of Advanced Materials (PRAMA) that allows us to present this work at the 12th International Symposium on Ultrafast Phenomena in Semiconductors (Vilnius, 22–25 August 2004).

References

- [1] *Terahertz Sources and Systems Electronics*, Eds. R. Miles, P. Harrison, D. Lip-pens, NATO Science Series II, Vol. 27, Kluwer Academic, Dordrecht 2001; *Sensing with Terahertz Radiation*, Ed. D. Mittleman, Springer Series in Optical Sciences, Vol. 85, Springer, Berlin 2003.
- [2] R.A. Chevillat, D. Grischkowsky, *Appl. Phys. Lett.* **67**, 1960 (1995).
- [3] J.D. Joannopoulos, R.D. Meade, J.N. Winn, *Photonic Crystals: Molding the Flow of Light*, Princeton University Press, Princeton 1995.
- [4] W. Robertson, G. Arjavalingam, R. Meade, K. Brommer, A. Rappe, J. Joannopoulos, *Phys. Rev. Lett.* **68**, 2023 (1992).
- [5] A. Chelnokov, S. Rowson, J.-M. Lourtioz, L. Duvillaret, J.-L. Coutaz, *Electron. Lett.* **33**, 1981 (1997).
- [6] L. Duvillaret, F. Garet, J.-L. Coutaz, *IEEE J. Select. Topics Quant. Electron.* **2**, 739 (1996).
- [7] P. Vincent, in: *Electromagnetic Theory of Gratings*, Ed. R. Petit, Springer Verlag, Berlin 1980.
- [8] L. Mashev, E. Popov, *Opt. Commun.* **55**, 377 (1985); G. Golubenko, A. Svakhin, V. Sychugov, A. Tishchenko, *Sov. J. Quant. Electron.* **15**, 886 (1985); A. Avrut-sky, V. Sychugov, *J. Mod. Opt.* **36**, 1527 (1989).
- [9] E. Bonnet, A. Cachard, A.V. Tishchenko, O. Parriaux, F. Garet, J.-L. Coutaz, G.A. Racine, in: *Conference on Microwaves and Terahertz Photonics, SPIE Pho-tonics Europe*, Strasbourg 2004, paper 5466-10.
- [10] J.-F. Roux, F. Aquistapace, F. Garet, L. Duvillaret, J.-L. Coutaz, *Appl. Opt.* **41**, 6507 (2002).
- [11] N. Katzenellenbogen, D. Grischkowsky, *Appl. Phys. Lett.* **61**, 840 (1992); T.-I. Jeon, D. Grischkowsky, *Appl. Phys. Lett.* **72**, 3032 (1998).
- [12] J.-L. Coutaz, L. Duvillaret, F. Garet, S. Rowson, A. Chelnokov, J.-M. Lourtioz, *SPIE Terahertz and Gigahertz Photonics* **3795**, 457 (1999).
- [13] F. Aquistapace, L. Duvillaret, F. Garet, J.-F. Roux, J.-L. Coutaz, *J. Appl. Phys.* **94**, 7888 (2003).